Interaction of two unequal corotating vortices

Interaction of two unequal corotating vortices

R. R. Trieling
Fluid Dynamics Laboratory, Department of Applied Physics, Eindhoven University of Technology, P.O. Box 513, 5600 MB Eindhoven, The Netherlands

O. U. Velasco Fuentes
Departamento de Oceanografía Física, CICESE, Ensenada, Baja California, Mexico

G. J. F. van Heijst
Fluid Dynamics Laboratory, Department of Applied Physics, Eindhoven University of Technology, P.O. Box 513, 5600 MB Eindhoven, The Netherlands

(Received 15 December 2004; accepted 14 June 2005; published online 29 July 2005)

Previous high-resolution contour dynamics calculations [Dritschel and Waugh, Phys. Fluids A **4**, 1737 (1992)] have shown that in two-dimensional inviscid flow the interaction of two unequal corotating vortices with uniform vorticity is not always associated with vortex growth and may lead to vortices smaller than the original vortices. In the present study, we investigate whether these results also hold for two-dimensional vortices with continuous vorticity distributions. Similar flow regimes are found as for uniform vorticity patches, but the variation of the flow regimes with the initial vortex radii and peak vorticities is more complicated and strongly dependent on the initial shape of the vorticity profile. It is found that the "halo" of low-value vorticity, which surrounds the cores of continuous vortices, significantly increases the critical distance at which the weaker vortex is destroyed. The halo also promotes the vortex cores to merge more efficiently, since it accounts for a substantial part of the loss of circulation into filaments. Simple transformation rules and merger criteria are derived for the inviscid interaction between two Gaussian vortices. The strong dependence of the flow regimes on the initial vorticity distribution partly explains why previous laboratory experiments in an electron plasma [Mitchell and Driscoll, Phys. Fluids **8**, 1828 (1996)] show complete merger of two unequal vortices in a range of parameter space where contour dynamics simulations with uniform vorticity patches predict partial merger or partial straining-out of the smaller vortex. It is shown that the measured times for complete merger are in reasonable agreement with inviscid dynamics when the vortices are very similar. For more distinct vortices the weaker vortex is often observed to be destroyed on a time scale much smaller than expected from inviscid numerical simulations. An explanation for this discrepancy is given by the combined effects of vortex stripping and viscous diffusion, which leads to an enhanced erosion of the weaker vortex. These results are verified by laboratory experiments in a conventional (rotating) fluid. © *2005 American Institute of Physics*. [DOI: 10.1063/1.1993887]

I. INTRODUCTION

The interaction of two like-signed vortices is a fundamental process in a variety of flow situations, ranging from aircraft wakes to geophysical flow systems, and has been the subject of intense research for the last three decades. Major attention has been given to the highly idealized configuration of two identical two-dimensional vortices. For this system three flow regimes have been identified.[1] For large initial separation the vortices rotate around each other endlessly, much in the same way as point vortices with identical circulation. At intermediate distances, the vortices rotate around each other while exchanging some vorticity, whereas at a distance smaller than a certain critical value the vortices merge into a single larger vortex surrounded by filamentary vorticity. The process of vortex merger is generally believed to be the most important mechanism of vortex growth in two-dimensional turbulent flows.

In practice, however, interactions will occur predominantly between vortices with different size and vorticity magnitude, and these unequal vortices may display different types of behavior. Indeed, high-resolution contour dynamics calculations by Dritschel and Waugh[2] (henceforth referred to as DW) have shown that the interaction of two differently sized vortex patches with equal uniform vorticity is much richer than that between two identical vortices. Depending on the initial separation distance and the initial ratio of vortex radii, five different flow regimes were identified. The definitions of these different flow regimes were based on the "efficiency" of the vortex interactions, which was quantified by computing the ratio of the final to initial circulation for each of the vortices. It was shown that the interaction between unequal vortices often results in two vortices, one of them being smaller than either of the original vortices, or in the complete destruction of the smaller vortex with no growth of the original larger vortex. Similar results were found in a related numerical study[3] for two differently sized vortices with unequal uniform vorticity.

The above-mentioned studies were limited to finite-area vortex patches with uniform vorticity and one may wonder whether the corresponding numerical results also hold for vortices with continuous vorticity distributions. In the present paper we will try to answer this yet unresolved question. The interaction of vortices with nonuniform vorticity may be significantly different from that of patches of uniform vorticity (i.e., Rankine vortices). For example, in an experimental study on interacting electron vortices, Mitchell and Driscoll[4] (henceforth referred to as MD) only found simple merger, i.e., the production of a single larger vortex, in regions of parameter space where DW found both a larger and a smaller vortex as a final state. Since the electron vortices were characterized by a continuous and smooth decrease of vorticity with radius, the vorticity distribution is a likely candidate to account for this discrepancy.

The dynamics of interacting vortices with distributed vorticity is highly relevant to two-dimensional turbulent flows. It has been recognized that the intermediate stage of freely decaying two-dimensional turbulence is dominated by well-separated vortex structures which vigorously interact once in a while during close encounters. Numerical simulations have shown that at moderate Reynolds number $Re[\sim O(1000)]$ these vortices can be well described by perturbed Gaussian vortices.[5] In order to capture the essential features of the dilute stage of freely decaying two-dimensional turbulence, Carnevale *et al.*[6] and Benzi *et al.*[7] formulated a modified point-vortex model in which spatially extended vortex structures are represented by point vortices. In this model, the point vortices are assumed to comply with Hamiltonian dynamics, except when two like-signed vortices come closer together than a critical separation distance at which stage the two point vortices are replaced instantaneously by a single point vortex. Since two point vortices cannot merge by definition, each vortex is represented by a typical vortex radius and vorticity magnitude, and simple transformation rules—based on the dynamics of vortices with uniform vorticity—are used to replace the two vortices by a single one. Although quantitative agreement was obtained with direct numerical simulations of the Navier–Stokes equations, it is still unclear whether these simple transformation rules and merger criteria are dynamically relevant to vortices with continuous vorticity distributions.

The effect of distributed vorticity on interacting vortices has not received much attention in the literature. In previous numerical studies[8,9] an initial configuration of two near patchlike vortices was considered, but this choice was merely made to accommodate the restrictions of the numerical model. Ehrenstrein and Rossi[10] determined equilibrium states of a pair of nonuniform vortices for several Gaussian-type initial vorticity profiles and also calculated for some specific cases the critical distance at which the equilibrium state loses stability (which may be a sign of the onset of vortex merger), but only one example of unequal vortices was considered. Using the same numerical procedure, Meunier *et al.*[11] derived a universal merger criterion for a pair of identical vortices, based on the second moment of vorticity as a characteristic measure of the vortex core size, which seemed to be applicable to a variety of vorticity distributions. A similar conclusion was drawn for finite-area vortices with continuous vorticity distribution in a related numerical study.[12] The question remains, however, whether this universal merger criterion is applicable to cases where the vortices are of unequal size and unequal vorticity magnitude.

In the present paper we study the effect of nonuniform vorticity on the interaction of two unequal corotating vortices. In Sec. II, we consider several vorticity distributions, ranging from top-hat to Gaussian shaped, and calculate the corresponding time evolution of the vortices based on the same numerical technique as used before by DW. In order to quantify the inelastic interaction process, a vortex census technique is used to isolate the vortex cores from the surrounding filamentary structures which enables calculation of the circulation in each of the final vortex cores. Since an investigation of full parameter space is a rather ambitious and elaborate task, attention is focused on two different cases. Inspired by previous numerical and experimental studies (DW and MD) we first consider interactions of two differently sized vortices with equal peak vorticity. In view of a complementary experimental study to be described in Sec. III of this paper we also investigate interactions of two vortices with different peak vorticities, but equal initial radii. In Sec. III, the laboratory experiments of MD are briefly reviewed and their results are compared with the contour dynamics results obtained in Sec. II. Laboratory experiments in a conventional (rotating) fluid enabled us to investigate the interaction of two unequal cyclonic vortices with different peak vorticities and approximately equal radii. In Sec. IV we discuss possible reasons for the discrepancy between laboratory experiments and numerical simulations. The main results are summarized and the conclusions are given in Sec. V.

II. NUMERICAL SIMULATIONS

A. Procedure

We examine the evolution of two initially circular vortices with either different size or different vorticity in a two-dimensional, inviscid, incompressible, homogeneous fluid. The initial vorticity distribution of each vortex is of the form

$$\omega(r) = \omega_0 \exp[-(r/a)^n], \tag{1}$$

where ω_0 is the peak vorticity, r is the distance to the vortex center, and n is a positive integer, being a measure of the steepness of the profile, ranging from $n=2$ (Gaussian profile) to infinity (top-hat profile). In this paper we define the vortex core radius R as the radius of maximum velocity. For the family of profiles considered the radius R is close to a (for example, $R=a$ for top-hat profiles and $R\approx 1.12a$ for Gaussian profiles). The vorticity profiles are shown in Fig. 1 for several values of the steepness parameter n. Each profile has been normalized by the peak vorticity ω_0 and the vortex core radius R. Most of the vorticity is concentrated in the vortex core, i.e., the region $r \leqslant R$, which is surrounded by a "halo" of low-amplitude vorticity.

The time evolution of the two-vortex system depends on five dimensionless parameters: (1) the initial ratio of vortex core radii, R_2/R_1, with R_1 and R_2 the initial radii of the larger and smaller vortex core, respectively, (2) the initial ratio of

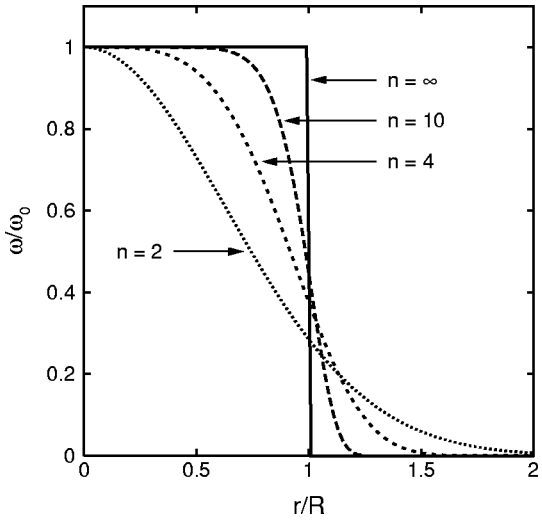

FIG. 1. Initial vorticity distributions according to Eq. (1) for several values of the steepness parameter n. Each profile has been normalized by the peak vorticity ω_0 and the radius of maximum velocity, R.

peak vorticities, ω_2/ω_1, with ω_1 and ω_2 the peak vorticities of the stronger and weaker vortex, respectively, (3) the normalized distance between the centers of the vortices, $d/\bar{R}$, with $\bar{R}=(R_1+R_2)/2$ the average radius of the two initial vortex cores, (4) the steepness parameter n_1 associated with the stronger vortex, and (5) the steepness parameter n_2 related to the weaker vortex. In addition, the interaction process may depend on the initial topological shape of the vortices, but in the present study only vortices with an initial circular shape are considered for simplicity. (Circular vortices are also believed to dominate moderate-*Re* two-dimensional turbulent flows due to the process of axisymmetrization.[13]) Both R_2/R_1 and ω_2/ω_1 are varied between 0.1 and 1.0, while $d/\bar{R}$ is varied within a variable range, and we restrict our attention to cases with $n_1=n_2=n$, with n ranging from 2 to ∞.

The two-vortex system is governed by the material conservation of vorticity,

$$\frac{D\omega}{Dt}=0, \tag{2}$$

where D/Dt is the material derivative for a two-dimensional scalar field advected by the local velocity $\mathbf{v}$, i.e., $D/Dt=\partial/\partial t+\mathbf{v}\cdot\nabla$, with ∇ the two-dimensional gradient operator. The vorticity ω and the velocity $\mathbf{v}$ are related to the streamfunction ψ by

$$\omega=-\nabla^2\psi, \tag{3}$$

and

$$\mathbf{v}=-\mathbf{k}\times\nabla\psi, \tag{4}$$

respectively, with $\mathbf{k}$ the unit vector perpendicular to the plane of motion. These equations are solved using the technique of contour dynamics.[14,15] The essence of contour dynamics is that the distribution of a piecewise-uniform vorticity field is completely determined by the instantaneous positions of the contours separating the different regions of uniform vorticity. The system can be integrated in time by advecting the contours with the local velocity (4). The latter follows directly from the inversion of Poisson's equation (3) with the piecewise-uniform vorticity field as a source. Hence we have a closed dynamical system for fluid particles that lie on the contours.

The contours are represented by a finite but adjustable number of nodes which are advected by the local velocity field. In general, the contours will be stretched and folded during the flow evolution, so that their length and curvature may increase considerably. Therefore, the number of nodes is allowed to change in time in response to possible deformations of the contours. The nodes are redistributed along the contours using cubic splines between the original nodes. In order to reduce the complexity of the contours and to be able to perform long-term time integrations, the technique of "contour surgery"[15] is applied. This technique removes dynamically unimportant contour features smaller than a prescribed length scale δ_s and reconnects contours enclosing the same value of vorticity when the contours get closer than this prescribed length scale. The surgical scale δ_s is equal to $\frac{1}{4}\mu^2 L$ where μL is approximately the maximum spacing between adjacent nodes on a contour, and L is a typical length scale characterizing the overall size of the coherent structures in the flow. All the calculations presented below were performed with $\mu=0.05$ and $L=R_1$ so that $\delta_s\sim 10^{-3}R_1$. Time integration was performed using a fourth-order Runge–Kutta method with a time step of $0.05(\omega_1)^{-1}$. The total area enclosed by the contours was conserved within 99%.

In the contour dynamics simulations of DW the velocity field was calculated by integrating the Green's function over the contours. For piecewise-vorticity distributions that involve a large number of contours the evaluation of these contour integrals is very time consuming. In the present study, a major reduction in computer time is achieved by application of the contour-advective semi-Lagrangian (CASL) algorithm.[16] This algorithm applies a contour-to-grid conversion to obtain the vorticity field on a fine-scale doubly periodic grid which is used to solve Poisson's equations by fast Fourier transforms to obtain the corresponding gridded velocity field. Bilinear interpolation is used to retrieve the velocity at the contours. The periodic boundary conditions did not significantly affect the vortex evolution (the size of the largest vortex core was less than 0.1 relative to the domain size). This was checked by doubling the size of the computational domain while keeping the same resolution, and by performing "traditional" contour dynamics simulations (without CASL) at strategically chosen positions in parameter space (e.g., close to the regime boundaries).

In order to initialize the contour dynamics calculations, it is necessary to discretize the continuous vorticity distribution of each vortex into a finite number of nested, uniform vorticity regions. The discretization is carried out in such a way that the discrete distribution of vorticity is closest to the continuous distribution in a least-squares sense, under the constraint that the circulation of the two distributions is the same (see Ref. 17 for details). Apart from Rankine vortices, which can be uniquely defined by a single contour, the vorticity distributions (1) are represented by 16 contours in order to resolve the "halo" of low-amplitude vorticity properly.

An additional contour of passive tracers was introduced to follow the evolution of the original vortex cores. Owing to the finite number of contours, the vorticity distributions (1) are effectively cut off at a radius corresponding to a vorticity level of approximately 1% of the maximum vorticity. Several contour dynamics simulations were repeated with twice the number of contours (and hence a larger cutoff radius), but no significant differences were observed.

B. Flow regimes

DW showed that the interaction of two differently sized vortices with equal uniform vorticity may be characterized by five flow regimes. In this paper, we use the same terminology as introduced by DW to identify the different flow regimes, but the definitions are slightly reformulated in order to deal with continuous vorticity distributions and to include interactions between equal-sized vortices with different vorticity magnitude:

(i) elastic interaction (EI): the vortex cores undergo small changes in shape but no vorticity is lost to filaments;
(ii) partial straining-out (PSO): part of the weaker vortex core is lost to filaments but no vorticity is entrained by the stronger vortex core;
(iii) complete straining-out (CSO): the weaker vortex core is completely torn apart but no vorticity is entrained by the stronger vortex core;
(iv) partial merger (PM): part of the weaker vortex core is removed and some of it is captured by the stronger vortex core;
(v) complete merger (CM): the weaker vortex core is completely destroyed and the final state consists of a single vortex core containing vorticity from the two original vortex cores.

The corresponding flow evolutions are shown in Fig. 2 for two interacting Rankine vortices. Note that the above definitions are fully consistent with those by DW for two differently sized vortices with equal uniform vorticity. It should also be stressed that these definitions apply to the evolution of the original vortex *cores* and not to the evolution of the far vorticity field, which in principle extends to infinity. If the definitions of the flow regimes would also involve the halo of low-amplitude vorticity, the flow evolution would always be classified as either partial or complete merger because vorticity, however small, is inevitably incorporated into the stronger vortex. For identical vortices it should be understood that "stronger" and "weaker" apply to each of the two vortices, and as a consequence only three regimes are relevant for identical vortices, i.e., elastic interaction, partial merger, and complete merger. (In previous numerical studies on the interaction of two identical vortices[1,18] these three regimes are referred to as "pulsation," "pulsation with exchange," and "merger," respectively.)

In order to identify the different flow regimes for two interacting Rankine vortices, DW quantified the efficiency of the interaction processes by computing the ratio of the final to initial circulation for each of the vortices. One major drawback of the quantitative analysis by DW is that some

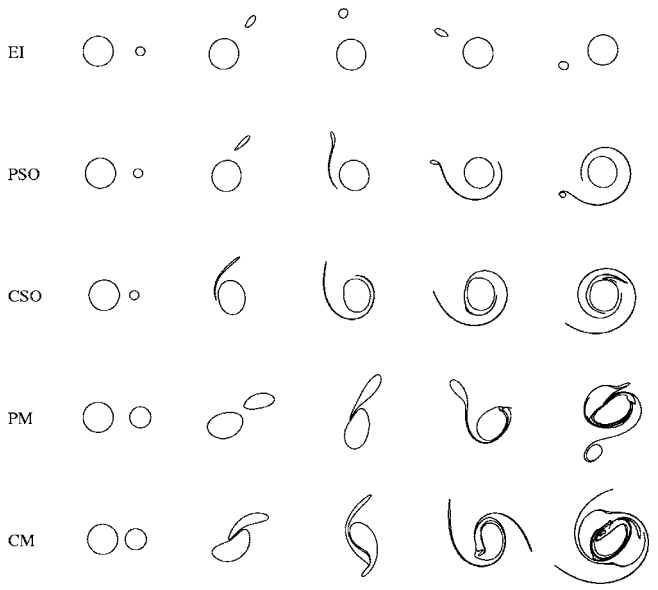

FIG. 2. Illustration of the five flow regimes defined by DW for two interacting Rankine vortices with equal vorticity magnitude. Elastic interaction (EI): $d/\bar{R}=4.3$, $R_2/R_1=0.3$. Partial straining-out (PSO): $d/\bar{R}=3.8$, $R_2/R_1=0.3$. Complete straining-out (CSO): $d/\bar{R}=3.1$, $R_2/R_1=0.3$. Partial merger (PM): $d/\bar{R}=3.3$, $R_2/R_1=0.7$. Complete merger (CM): $d/\bar{R}=2.6$, $R_2/R_1=0.7$.

vortex interactions may be erroneously assigned to a specific flow regime. For example, at intermediate distances, e.g., $d/\bar{R}=3.4$, two identical vortices with uniform vorticity rotate around each other while periodically exchanging a substantial amount of vorticity (see also Ref. 19). According to the qualitative definitions of the flow regimes, this interaction process should be classified as partial merger. DW, however, classified this interaction process as elastic interaction because after each exchange of vorticity the vortices have virtually the same circulation as initially. A similar misinterpretation may occur for unequal vortices, e.g., when the net exchange of circulation between the stronger and the weaker vortex is zero (or within the numerical error of determining the circulation of each vortex core). Therefore, in the present study, the different flow regimes are identified based upon a visual inspection of the interaction events. The flow evolution was monitored for at least 10 eddy turnover times until a (transient) stable state was observed. At this stage the interaction process was assigned to one of the five flow regimes.

Figure 3 shows the flow regimes corresponding to $\omega_1=\omega_2$ (left column) and $R_1=R_2$ (right column) for several initial vorticity distributions, ranging from Rankine to Gaussian-type: (a) and (d) $n=\infty$, (b) and (e) $n=4$, (c) and (f) $n=2$. All interaction scenarios could be characterized by one of the five flow regimes defined above. For each initial vorticity distribution the regimes are indicated by different symbols in two-dimensional parameter space spanned by the initial separation distance $d/\bar{R}$ and either the initial ratio of core radii R_2/R_1 or the initial ratio of peak vorticities ω_2/ω_1. (Note that in all cases the vortex cores touch when $d/\bar{R}=2$.) The solid curves indicate the approximate locations of the

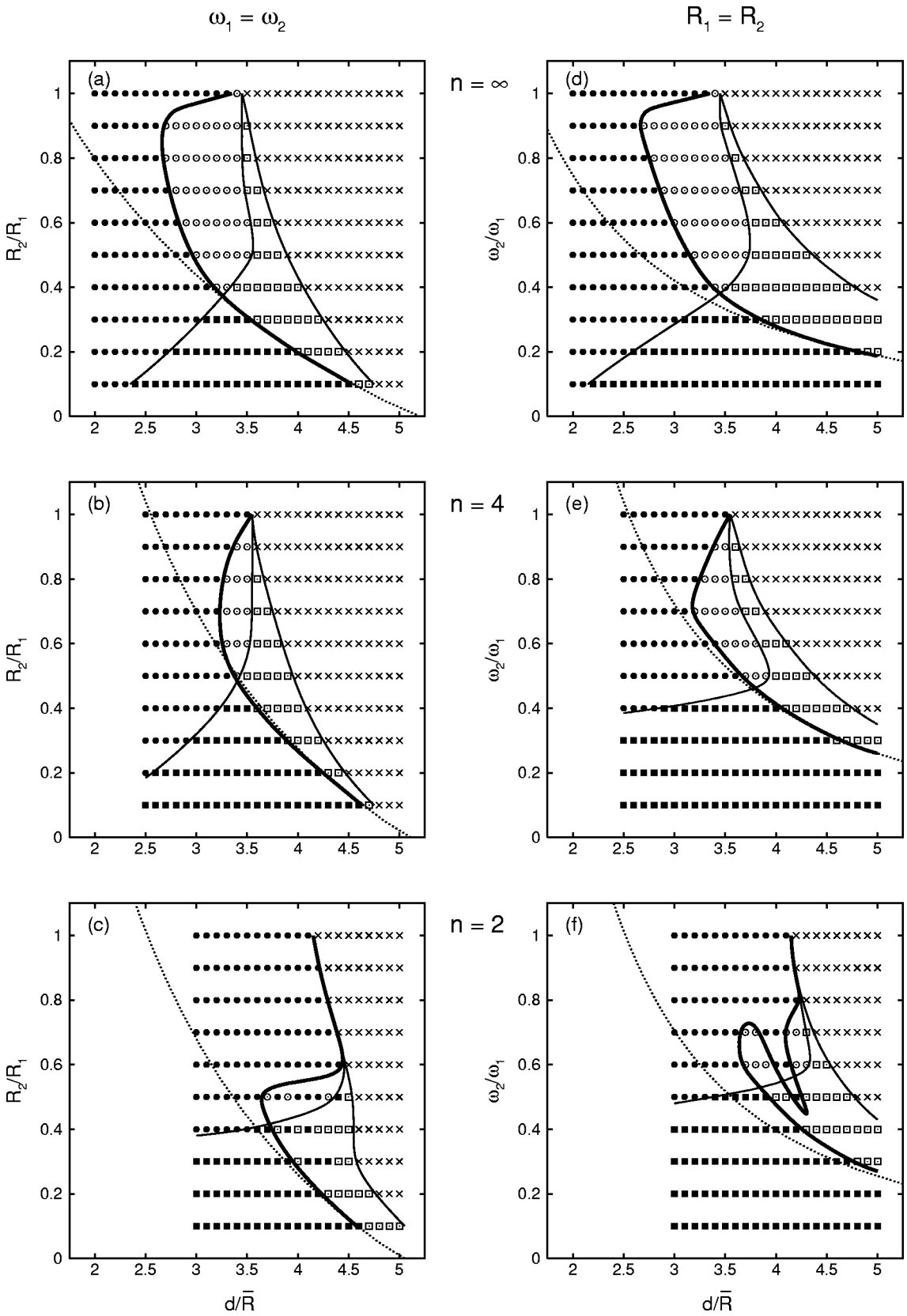

FIG. 3. Flow regimes for equal-vorticity interactions (left column) and equal-radii interactions (right column) with (a), (d) $n=\infty$, (b), (e) $n=4$, and (c), (f) $n=2$. The flow regime is indicated for each initial condition with R_2/R_1 the initial ratio of vortex core radii, ω_2/ω_1 the ratio of peak vorticities, and $d/\bar{R}$ the initial separation distance. Elastic interactions are represented by a cross (×), partial straining-out by an open square (□), complete straining-out by a filled square (■), partial merger by an open circle (○), and complete merger by a filled circle (●). The solid lines indicate the boundaries between the regimes, whereas the dotted line corresponds to the predicted boundary between complete straining-out and partial straining-out based on local strain arguments. The critical boundary is indicated by the thick solid line.

boundaries between the regimes. The thick solid curve is special because it marks the boundary at which the weaker vortex is completely destroyed. This critical boundary thus separates flow evolutions resulting in one and two final vortices, respectively.

We first focus on Figs. 3(a)–3(c), which represent interactions between vortices with equal vorticity magnitude but different core radii. Figure 3(a) corresponds to the case previously investigated by DW. Comparison with Figs. 3(b) and 3(c) shows that the regions associated with partial merger and partial straining-out become significantly smaller with increasing smoothness of the vorticity profile, i.e., with decreasing n in (1). For Gaussian vortices these flow regimes apparently vanish for vortices of similar size ($R_2/R_1 > 0.6$). The complete merger regime is shifted toward larger separation distances, especially for Gaussian vortices of similar size, while complete straining-out events become more important at larger ratios R_2/R_1.

Looking at Figs. 3(a) and 3(b) we see that for each value of R_2/R_1 the smaller vortex is always completely torn apart if the initial separation distance $d/\bar{R}$ is smaller than some critical value $(d/\bar{R})_c$. For separations above this critical value the smaller vortex always survives. In these cases the critical boundary can thus be described by a functional relationship of the form $d_c = f(R_2/R_1)$. For Gaussian vorticity profiles ($n = 2$), however, the transition between flow regimes associated with one and two final vortices is much more complicated and a single critical distance cannot be defined for all R_2/R_1, see Fig. 3(c). This result is persistent at least up to 20 eddy turnover times. Due to a lack of spatial resolution in parameter space, the regime diagram in Fig. 3(c) is not conclusive about whether each flow regime should form a simply connected region or a collection of multiple isolated regions. For that reason we have only marked the approximate position of the boundary below which the smaller vortex is always completely destroyed. In regions of parameter space where several flow regimes appear to coexist, the fate of the smaller vortex core was observed to be very sensitive to transient interactions with nearby filamentary debris that originated from the extended halo of low-amplitude vorticity. These transient interactions may be the likely cause for the complex structure of the critical boundary.

In Figs. 3(d)–3(f) we show the flow regimes for the same initial vorticity distributions, but now the vortices have equal radii $R_1 = R_2$ while the ratio of maximum vorticities is varied. The topology of the regime diagrams is very similar to that in Figs. 3(a)–3(c). The regions associated with partial merger and partial straining-out again become smaller with increasing smoothness of the vorticity profiles. Likewise, for Gaussian vortices the critical boundary is more complicated than for vortices with steeper vorticity profiles. It has a conspicuous folded structure at intermediate values of ω_2/ω_1, which makes it impossible to define a single critical distance for all values of ω_2/ω_1.

For vortices with significantly different size or vorticity magnitude, i.e., relatively small R_2/R_1 or ω_2/ω_1, the position of the critical boundary can be understood by considering the weaker vortex in the adverse shear induced by the stronger vortex. It is known from previous analytical and numerical studies[20–22] that an initially circular vortex with uniform or peak vorticity ω_0 will be irreversibly torn apart in adverse shear if the strain rate of the shear, γ, is larger than some critical value $\gamma_c = \beta_n \omega_0$, with β_n a constant depending on the initial shape of the vorticity profile. For uniform vortices, we expect the weaker vortex to be destroyed by the stronger vortex when the entire weaker vortex is subject to the condition $\gamma > \gamma_c$ (see also DW). For nonuniform vortices the same condition for irreversible tearing is expected to apply, but now at the center of the weaker vortex. In order to determine β_n, additional contour dynamics simulations were carried out with a single vortex in adverse shear for various values of the steepness parameter n. The dotted lines in Fig. 3 indicate the critical distance at which the weaker vortex (either with smaller radius or smaller vorticity amplitude) is expected to be destroyed and a close agreement is obtained with the boundary between partial straining-out and complete straining-out particularly for small R_2/R_1 and ω_2/ω_1.

The above approximation fails for larger values of R_2/R_1 and ω_2/ω_1 due to spatial variation of the shear across the weaker vortex and the fact that the shear induced by the stronger vortex increases when it captures vorticity removed from the weaker vortex. Also shape deformations of the stronger vortex may seriously affect the shear it induces. In this region of parameter space it appears that for Gaussian vortices the transition to complete merger can be closely approximated by $d/\bar{R} = \delta$, with $\delta = 4.15(\pm 0.05)$ the critical distance for two identical Gaussian vortices, especially when we neglect the detailed structure of the critical boundary, see Fig. 4. A similar criterion was suggested by Carnevale *et al.*[6] and Benzi *et al.*[7] to transform two differently sized vortices with equal vorticity into a single new vortex, but in their case δ was based on the critical distance of two equal Rankine vortices. Figure 3(a) shows that this criterion fails to model the critical distance of Rankine vortices properly since the latter is strongly dependent on R_2/R_1. The criterion is also too strict to model the critical boundary for Gaussian vortices. The present study reveals that the criteria defined by Carnevale *et al.*[6] and Benzi *et al.*[7] may improve remarkably by simply taking $\delta = 4.15$. For small values of R_2/R_1 and ω_2/ω_1 the criterion should still be based on the vortex-in-shear argument, although for equal-vorticity interactions only a small error is made when the condition $d/\bar{R} = 4.15$ is used, see Fig. 4.

As we have seen in Fig. 3, the critical distance increases significantly with decreasing steepness parameter n, especially for small values of n. This increase may be attributed either to the variation of the vorticity distribution inside the vortex core, or to the spatial extent of the halo of low-amplitude vorticity, or to both. Therefore, the numerical calculations were repeated for Gaussian vortices ($n = 2$) but with the halo of each vortex being removed, which was easily feasible from a numerical point of view by just removing the outer seven contours of each of the original vortices. Figure 5 shows the flow regimes (symbols) and the flow regime boundaries (solid lines) of the interaction of two Gaussian vortices without halos. Comparison of Figs. 3(c) and 3(f)

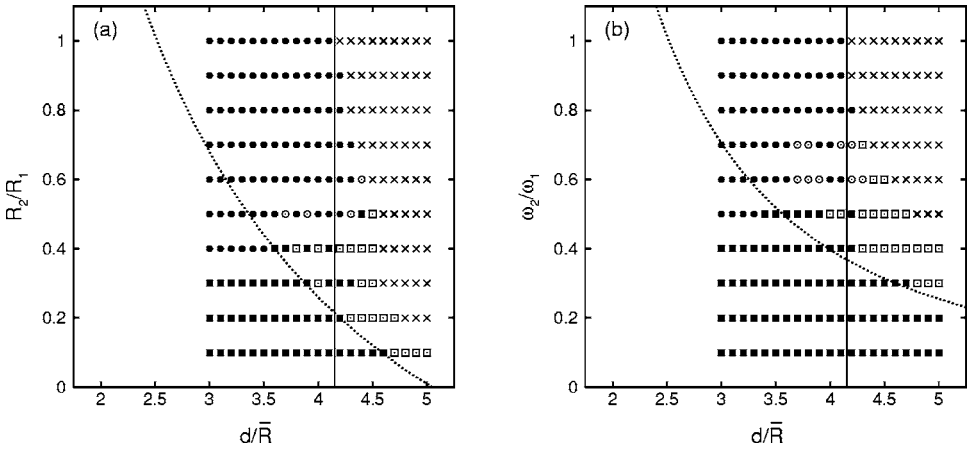

FIG. 4. Flow regimes for $n=2$: (a) $\omega_1=\omega_2$, (b) $R_1=R_2$. The symbols have the same meaning as in Fig. 3. The solid line corresponds to the merger criterion $d/\bar{R}=\delta$, with $\delta=4.15$, whereas the dotted line corresponds to the predicted boundary between complete straining-out and partial straining-out based on local strain arguments.

with Figs. 5(a) and 5(b) proves that the absence of the halo makes a major difference in the regime diagram. On the other hand, comparison between the regime boundaries of the Gaussian vortices without halos (solid lines in Fig. 5) and the regime boundaries associated with two interacting Rankine vortices (dashed lines in Fig. 5) shows that changing the vorticity distribution within the Gaussian vortex cores has little effect. Therefore, we may conclude that it is the halo of low-level vorticity, and not the vorticity distribution inside the core, that is the cause of the significant increase of the critical distance with decreasing steepness of the vorticity profile. (This observation supports the use of Rankine vortices in high-resolution numerical simulations of nearly inviscid two-dimensional turbulence[23] since in the inviscid limit distributed vortices can easily be stripped of their halo.[24]) When the vorticity profiles (1) are cut off at radii corresponding to vorticity values much less than 1% of the maximum vorticity, the regime boundaries were observed to be virtually unaffected, indicating that the halo may be considered passive for vorticity values smaller than 1% of the maximum vorticity.

In their attempt to define a universal merger criterion for a pair of identical vortices, Meunier *et al.*[11] suggested to use an alternative definition of the vortex core radius, which was defined as the square root of angular impulse divided by the circulation. This definition has some advantages over our definition of the vortex core since it is a conserved quantity in inviscid flow that can be applied unambiguously to any vorticity distribution of any topological shape. The critical distance, normalized with this alternative definition of the vortex core, appeared to be much less sensitive to the initial vorticity profile in the case of two identical vortices. It is interesting to examine whether this critical distance is also universal for unequal vortices. In Fig. 6 the critical boundaries corresponding to four different initial vorticity distributions ($n=2$, 4, 10 and ∞) are plotted together in a single graph for (a) $\omega_1=\omega_2$ and (b) $R_1=R_2$. The separation distance is normalized in the same way as was done by Meunier *et al.*[11] For identical vortices the variation of the critical distance with n is indeed very small, but for unequal vortices we observe a significant dependence on the initial vorticity profile. Despite the benefits of a moment-based definition of the vortex core radius, it clearly does not lead to a collapse of the critical boundaries for unequal vortices.

C. Quantification of the interaction process

As we have seen in Fig. 2, inelastic interactions between two vortices may lead to vortices differing in circulation from either of the original vortices. For each of the two vortex cores the gain or loss of circulation is quantified by calculating the ratio of the final to initial circulation according to

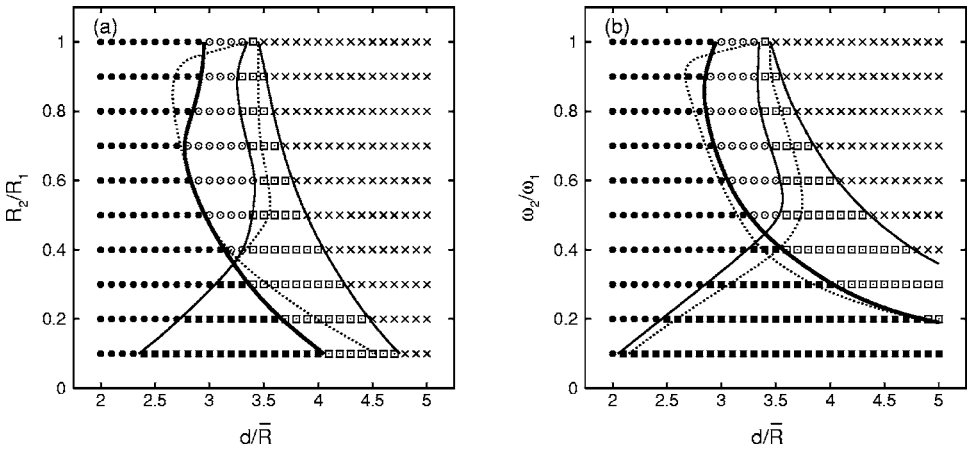

FIG. 5. Flow regimes for $n=2$, but with the vorticity distribution being cut off at $r=0.96R$: (a) $\omega_1=\omega_2$, (b) $R_1=R_2$. The symbols and lines have the same meaning as in Fig. 3 except for the dotted lines which represent the regime boundaries associated with two interacting Rankine vortices.

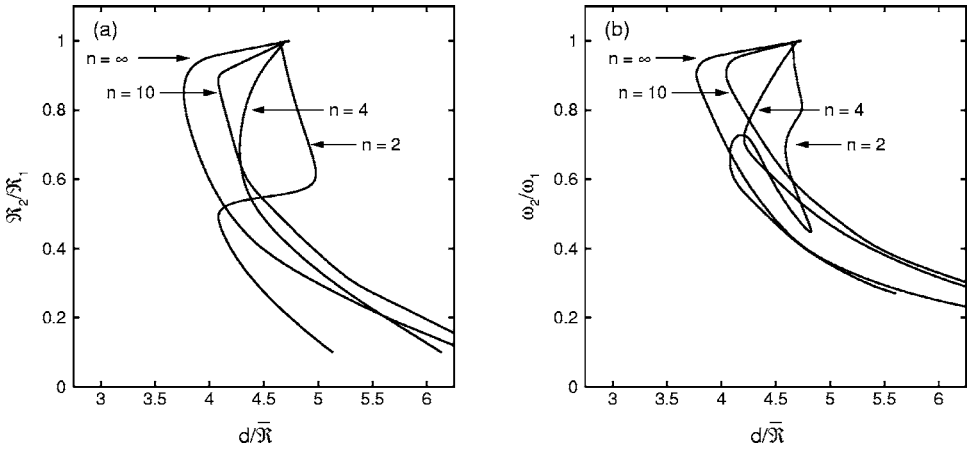

FIG. 6. Boundaries between regimes associated with one and two final vortices, respectively. The results of four different initial vorticity distributions ($n=2$, 4, 10 and ∞) are plotted together in a single graph for (a) $\omega_1=\omega_2$ and (b) $R_1=R_2$. The vortex core radii $\mathcal{R}_1,\mathcal{R}_2$ and $\bar{\mathcal{R}}$ are based on the second moment of vorticity (see Meunier *et al.*, Ref. 11).

$$\epsilon_1=\frac{\Gamma_{1f}}{\Gamma_{1i}},\quad \epsilon_2=\frac{\Gamma_{2f}}{\Gamma_{2i}}, \tag{5}$$

where the subscripts i and f refer to the initial and final states of the evolution, and Γ_1 and Γ_2 represent the circulation bound in the cores of the stronger and the weaker vortex, respectively. Owing to the formation of filamentary vorticity, the total circulation in the final vortex cores is generally less than the total circulation in the initial vortex cores. In order to quantify this net loss of circulation to filaments, we define

$$\mathcal{E}=\frac{\Gamma_{1f}+\Gamma_{2f}}{\Gamma_{1i}+\Gamma_{2i}}, \tag{6}$$

which represents the fraction of the initial circulation $\Gamma_{1i}+\Gamma_{2i}$ bound in the final vortex cores, see also Ref. 1.

Before we can apply the above definitions to inelastic interactions we need to identify the vortex cores in the final vorticity distribution. DW used a "coarse-graining" procedure (see also Ref. 1) to isolate the resultant vortices from the surrounding filamentary structures by repeatedly increasing the surgical scale. In this way, the small-scale structures were removed while the large-scale structures were virtually unaffected. Although this procedure can in principle be applied to nonuniform vortex cores, we should be aware that the resulting coherent structures may not necessarily correspond to the cores of the newly formed vortices. In other words, the cores of the final vortices may contain fluid from both the original vortex cores and the original halos of low-amplitude vorticity. For that reason, we have adopted an alternative approach. According to Weiss[25] we can define a function $Q=\mathrm{tr}[(\nabla\mathbf{v})^2]$ which is proportional to the rate of strain squared, S^2, minus the vorticity squared, ω^2, i.e., $Q=\frac{1}{2}(S^2-\omega^2)$. [Note that with the incompressibility condition $\nabla\cdot\mathbf{v}=0$, it follows that $Q=-2\det(\nabla\mathbf{v})$.] The Weiss function Q appears to be a convenient measure to distinguish between the vortex core and the halo of filamentary features. Regions with positive Q, i.e., $|S|>|\omega|$, are characterized by structures that are dominated by strain, such as vorticity filaments, whereas regions with negative Q, i.e., $|S|<|\omega|$, are related to structures that are dominated by rotation, such as coherent vortices. Motivated by the fact that for axisymmetric vortices Q changes sign where the azimuthal velocity reaches a maximum, we associate each region of negative Q with a vortex core. This choice is consistent with our definition of the vortex core radius R. Since the streamfunction and vorticity field were already available as a byproduct of the CASL algorithm, the Weiss function could be easily calculated using finite differences. A simplified version of the vortex census technique introduced by McWilliams[26] was used to reject irrelevant features with negative Q that were clearly not associated with the vortex core. In general, both the coarse-graining procedure and the Weiss function approach yielded very similar results. From this observation it may be concluded that the final vortex cores are almost entirely formed by fluid originating from the initial vortex cores. For that reason, we will only discuss the results from the coarse-graining procedure. Also, in the following analysis we will only focus on equal-vorticity interactions since the interactions between equal-sized vortices with different vorticity yielded qualitatively similar results.

Figure 7 shows the variation of ϵ_1,ϵ_2, and $\mathcal{E}$ with initial distance $d/\bar{R}$ for different values of R_2/R_1 and n. The time at which the circulation within the final vortex cores was quantified corresponds to the same stage at which the interaction process was assigned to one of the five flow regimes. The symbols have the same meaning as in Fig. 3. Within the partial merger and complete merger regimes there is a general trend for the circulation of the larger resultant vortex core to increase with decreasing separation distance, see Figs. 7(a)–7(c). Thus the closer the initial vortex cores are together, the more circulation is entrained by the larger vortex core. For identical Rankine vortices, however, this general trend sets in only after reaching the local minimum around $d/\bar{R}=2.9$. We also observe that the circulation of the larger resultant vortex core increases monotonically with R_2/R_1. This is a direct consequence of the fact that the maximum circulation that can be captured by the larger vortex core is proportional to the area of the smaller initial vortex core. Within the partial merger or partial straining-out regimes, the circulation of the smaller resultant vortex core generally decreases with decreasing separation distance until it becomes zero in the complete merger or complete straining-out regimes, see Figs. 7(d)–7(f). The variation of $\mathcal{E}$ with $d/\bar{R}$ is shown in Figs. 7(g)–7(i), which reveal that for each R_2/R_1 the fraction of the initial core circulation cap-

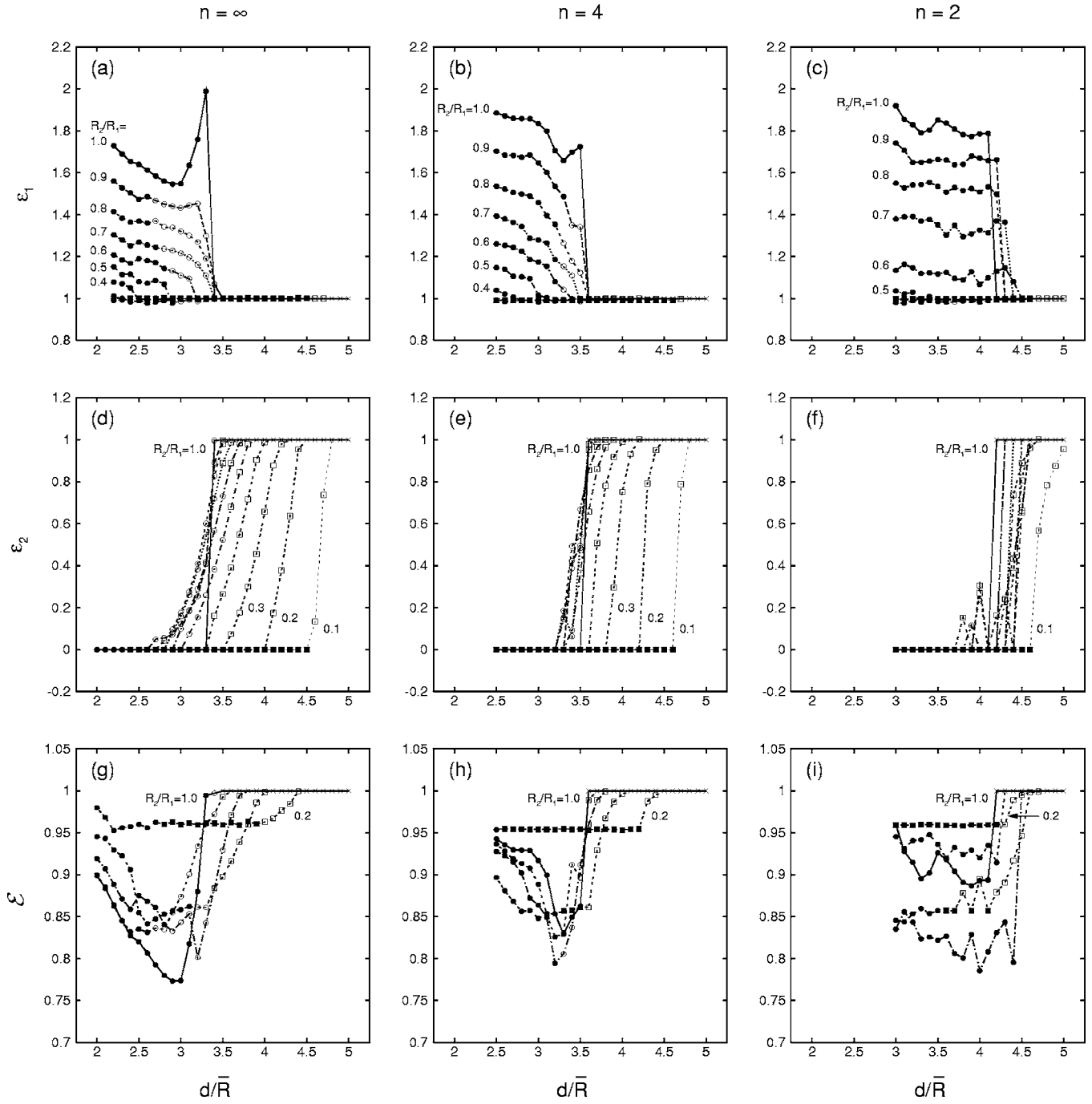

FIG. 7. Variation of ϵ_1 [panels (a)–(c)], ϵ_2 [panels (d)–(f)], and $\mathcal{E}$ [panels (g)–(i)] with initial separation distance $d/\bar{R}$ for ω_2/ω_1=1.0 and different values of R_2/R_1 and n. The different line styles correspond to different values of R_2/R_1. The symbols have the same meaning as in Fig. 3. For clarity only data points associated with the even ratios R_2/R_1 are shown in panels (g)–(i).

tured by the final vortex cores reaches a minimum close to the critical distance $(d/\bar{R})_c$. In all cases, at least 75% of the initial core circulation remains bound in the final vortex cores.

The gain or loss of circulation depends strongly on the initial vorticity profile, which is clear from a direct comparison of cases with different steepness parameter n and the same ratio R_2/R_1, see Fig. 8 for $R_2/R_1=0.8$. For complete merger and partial merger events, the circulation captured by the larger final vortex core is significantly larger for smoother vorticity profiles. In particular, for Gaussian vortices the circulation of the larger final vortex core reaches an almost optimal value, indicated by the horizontal dotted line in Fig. 8. This strong dependence on the vorticity profile may be explained by the general observation that the vorticity filaments are expelled from the periphery of each vortex. The circulation removed from each vortex core therefore may depend crucially on the spatial extent of the halo of low-amplitude vorticity. For example, consider the complete merger events for the three different initial vorticity distributions shown in Fig. 9: (a) $n=\infty$, (b) $n=4$, and (c) $n=2$, all with $R_2/R_1=0.8$. The dark-shaded areas correspond to the

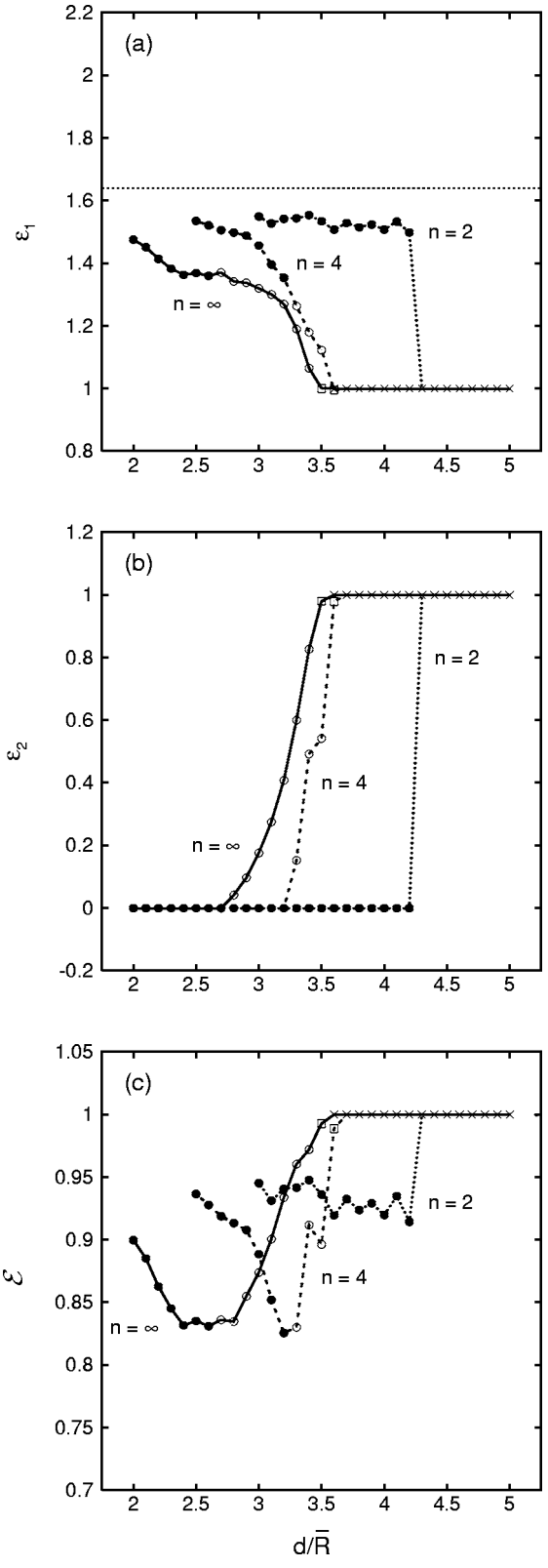

FIG. 8. Variation of (a) ϵ_1, (b) ϵ_2, and (c) $\mathcal{E}$ with initial separation distance $d/\bar{R}$ for $R_2/R_1=0.8$ and $\omega_2/\omega_1=1.0$ and different values of n. The different line styles correspond to different values of n. The symbols have the same meaning as in Fig. 3. The horizontal dotted line corresponds to the optimal value of ϵ_1 for this case.

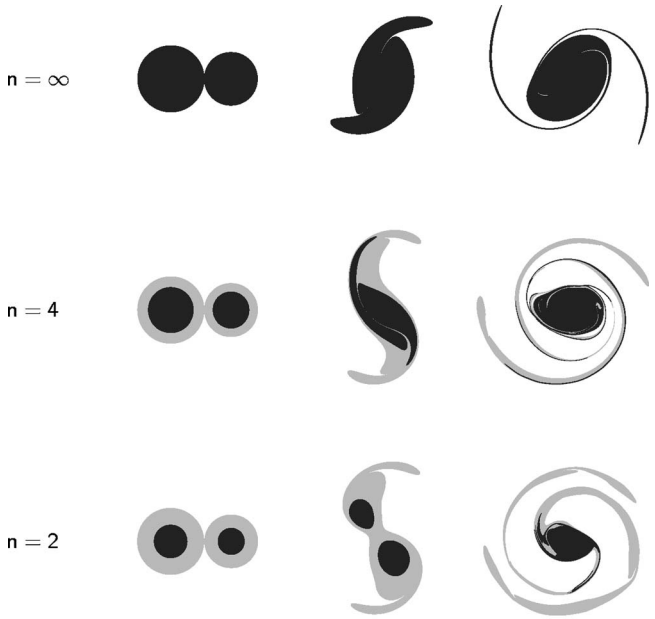

FIG. 9. Illustration of the loss of circulation into filaments for three different initial vorticity distributions: (a) $n=\infty$ (with $d/\bar{R}=2.0$), (b) $n=4$ (with $d/\bar{R}=2.9$), and (c) $n=2$ (with $d/\bar{R}=3.0$), all with $R_2/R_1=0.8$ and $\omega_2/\omega_1=1.0$. The dark-shaded area corresponds to the core of the initial vortex, whereas the light-shaded area corresponds to the halo of the initial vortex.

initial core region of each vortex, whereas the light-shaded areas correspond to the halo of low-amplitude vorticity exterior to the initial vortex cores. The vortex edge corresponds to the outermost contour of the discretized vorticity distribution. In each case, vorticity filaments are shed from the edge of each vortex and, as remarked before, the newly formed vortex core mainly consists of fluid that originates from the initial vortex cores. However, the composition of the filaments is notably different in each case. For Rankine vortices, the filaments are necessarily expelled from the vortex cores as the vortices have no halo. For smoother vorticity profiles, a substantial part of the filamentary vorticity is drawn from the halo of low-amplitude vorticity and hence more circulation of the original vortex cores is available to form the final vortex core. For Gaussian vortices, the filaments are expelled almost entirely from the halo of low-amplitude vorticity and the vortex cores merge almost without loss of circulation. Taken together, the halo of low-amplitude vorticity has an important impact on the gain or loss of circulation within the vortex cores.

Figure 8 also shows that the circulation of both the smaller and larger final vortex core changes much faster with separation distance near the critical boundary for smoother vorticity distributions. This may be explained by our previous observation that the regions associated with the partial merger and the partial straining-out regimes become significantly smaller with increasing smoothness of the vorticity profile, see Fig. 3. For Gaussian vortices both ϵ_1 and ϵ_2 and consequently $\mathcal{E}$ change almost abruptly near the critical boundary since at the corresponding ratios R_2/R_1 the vortex cores either merge almost perfectly or they interact elastically.

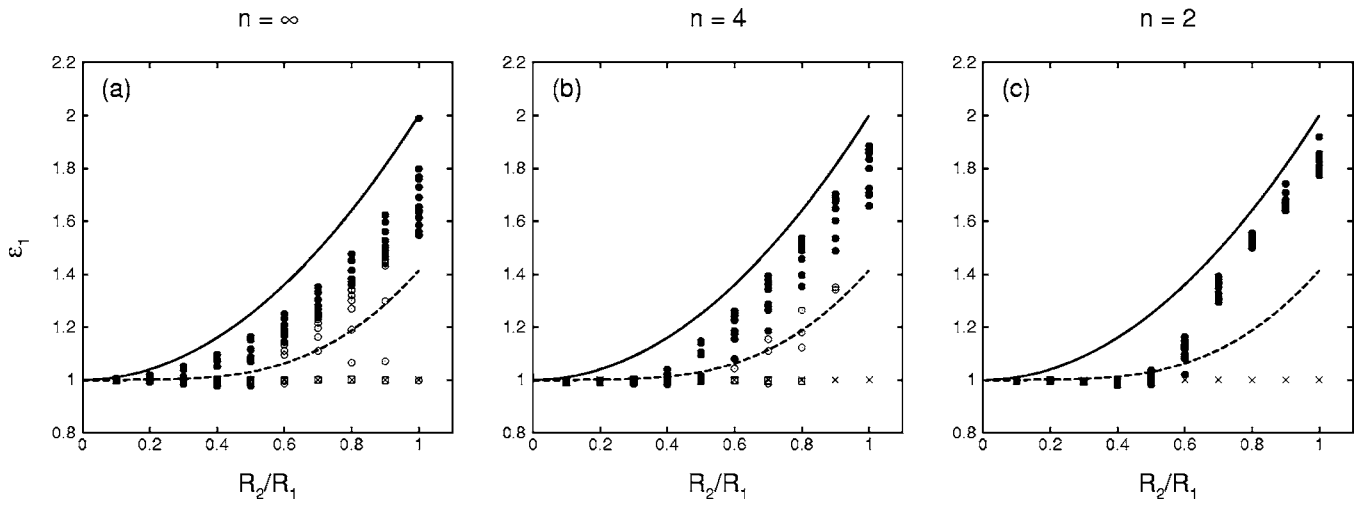

FIG. 10. Ratio of the final to initial circulation bound in the core of the larger vortex as a function of the ratio R_2/R_1 for equal-vorticity interactions: (a) $n=\infty$, (b) $n=4$, and (c) $n=2$. The symbols have the same meaning as in Fig. 3. The dashed line corresponds to the results by Carnevale *et al.* (Ref. 6) and Benzi *et al.* (Ref. 7), whereas the solid line corresponds to the alternative transformation rule based on the conservation of total initial circulation in the vortex cores.

In Fig. 10 we again show the ratio of circulation bound in the larger vortex core but now as a function of the ratio R_2/R_1 for different values of $d/\bar{R}$ and n. This allows us to make a comparison with the transformation rule for complete merger formulated independently by Carnevale *et al.*[6] and Benzi *et al.*[7] When two vortices with the same vorticity come closer together than a critical separation distance, the transformation replaces the two vortices with a single vortex of radius $R=(R_1^4+R_2^4)^{1/4}$, where R is the radius of the newly formed vortex core. This implies that $\epsilon_1=[1+(R_2/R_1)^4]^{1/2}$ (dashed lines in Fig. 10) and $\epsilon_2=0$. Clearly, the above parametrization does not take into account that the size of the resultant vortices varies with the separation distance $d/\bar{R}$ and that inelastic interactions may produce one larger and one smaller vortex. The former is evident from the large amount of scatter in Fig. 10, especially for steep vorticity profiles. In all cases, the transformation rule clearly underestimates the circulation bound in the larger final vortex core. Given the fact that Gaussian vortices are representative of the vortices in moderate-*Re* two-dimensional turbulent flows[5] and that their vortex cores merge almost without loss of circulation it seems appropriate to use an alternative transformation rule based on the conservation of the total initial circulation in the vortex cores, i.e., $R^2=R_1^2+R_2^2$, which implies that $\epsilon_1=[1+(R_2/R_1)^2]$ (solid lines in Fig. 10) and $\epsilon_2=0$. Indeed, for Gaussian vortices of not too different size, the data points in Fig. 10(c) associated with complete merger are located much closer to the curve corresponding to the alternative transformation rule. A similar transformation rule, based on the conservation of the total core circulation, applies to vortices with different peak vorticity and equal radii, i.e., $\epsilon_1=[1+(\omega_2/\omega_1)]$.

III. LABORATORY EXPERIMENTS

In this section, laboratory experiments are described in order to verify the numerical results for two unequal vortices with nonuniform vorticity. Two different cases are considered: (a) vortices with different radii but equal peak vorticity, and (b) vortices with different peak vorticity and equal radii. The first case has been previously investigated in confined electron plasmas by MD, while the second case was investigated in the present study by performing laboratory experiments in a conventional (rotating) fluid.

A. Electron-plasma experiments

MD investigated the interaction between two electron plasma columns inside hollow conducting cylinders subjected to an axial magnetic field. In the range of experimental parameters considered, these columns were found to evolve as two-dimensional vortices in an incompressible nearly inviscid fluid. Figure 11 shows the measured radial vorticity profiles (indicated by the symbols) together with four members of the family of vorticity profiles (1), i.e., $n=2$, 4, 10

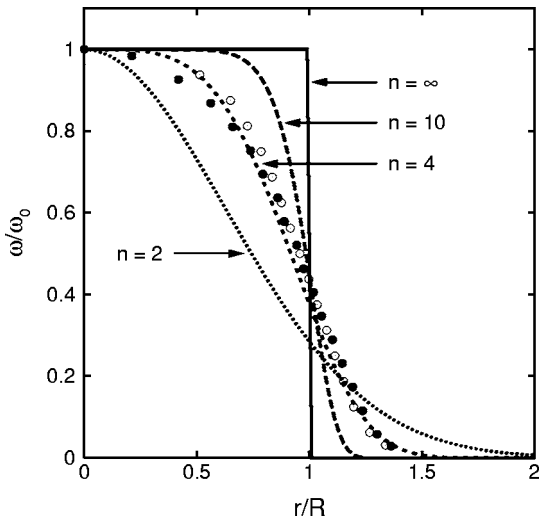

FIG. 11. Radial distributions of vorticity for two confined electron vortices with $R_2/R_1=0.67$, as obtained by MD. The circles and bullets correspond to the smaller and the larger vortex, respectively. The curves represent the vorticity distributions given by Eq. (1) for different values of n.

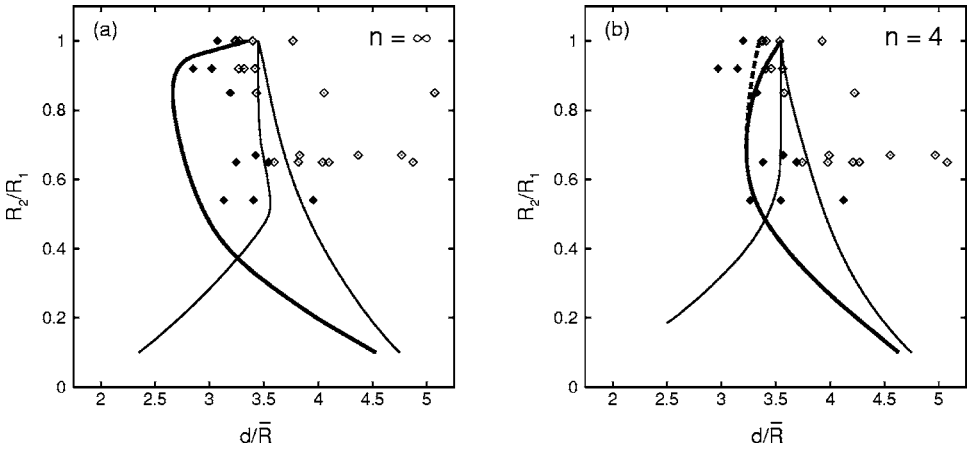

FIG. 12. Comparison between the numerically obtained flow regimes for equal-vorticity interactions ($\omega_1=\omega_2$) and the results by MD: (a) $n=\infty$ and (b) $n=4$. Filled symbols indicate merger in less than one orbit period; open symbols indicate merger in more than one orbit period. The solid lines represent the boundaries between the numerically obtained regimes (the critical boundary is indicated by the thick solid line) and are identical to those in Fig. 3. The dashed line represents the isocurve for complete merger (or complete straining-out) in about one orbit period. (For $n=\infty$ the dashed line is obscured by the thick solid line.)

and ∞. The measured vorticity profiles have been retrieved from Fig. 16 of Ref. 4. The electron vortices are characterized by a continuous and smooth decrease of vorticity with radius and are close to the vorticity profile with $n=4$. MD performed a series of laboratory experiments in which the profile and the peak vorticity of the initial vortices were nearly the same, while the radii and initial separation were varied. In contrast to what might be expected from the regime diagram in Fig. 3(b), which corresponds to equal-vorticity interactions with $n=4$, only complete merger events were observed with the electron vortices. The plasma experiments showed no clear evidence of interactions leading to a stable configuration of both a larger and a smaller vortex.

Although dissipation was very low in the electron-plasma experiments, we have to keep in mind that in any viscous situation vortices will expand radially outward. This implies that a stable configuration of two final vortices will never be established and that the vortex interaction will ultimately lead to a single vortex, whatever the initial separation distance $d/\bar{R}$ (see Ref. 18). Indeed, the interaction between electron vortices always led to complete merger in the long run. [Complete straining-out events were not observed because the initial conditions were limited to $R_2/R_1 \geqslant 0.5$, see Fig. 3(b).] Therefore, with viscous dissipation present, the question is not if, but rather when the final stage of a single vortex is reached. For vortex interactions that do not lead to a single vortex in the inviscid case, we expect the smaller vortex to be destroyed on a viscous time scale large compared to the convective time scale at which inviscid interactions usually take place. For the electron-plasma experiments we may therefore distinguish between complete merger on a convective time scale and complete merger on a viscous time scale, and we expect that these two flow scenarios are separated by the critical boundary for inviscid interactions.

Although it is rather arbitrary to determine precisely where the distinction between the convective and the viscous time scales should be made, MD distinguished between complete merger in less than one orbit and complete merger in more than one orbit. This choice appears to be a reasonable one since the contour dynamics simulations described in Sec. II reveal that complete merger events generally occur within one orbit period. This is confirmed by Fig. 12, which shows the regime boundaries for inviscid interactions with (a) $n=\infty$ and (b) $n=4$ (solid lines), together with the isocurves for complete merger (or complete straining-out) in about one orbit (dashed lines). These isocurves closely coincide with the corresponding critical boundaries (thick solid curves) except for similar-sized vortices with $n=4$ [see Fig. 12(b)]. The initial conditions of the electron-plasma experiments are indicated by the markers in Fig. 12. Filled symbols indicate complete merger in less than one orbit period, and open symbols indicate complete merger in more than one orbit period. A comparison with the numerical results for Rankine vortices, Fig. 12(a), reveals that many complete mergers occur on a convective time scale where complete mergers on a viscous time scale are expected. This observation was also noted by MD. Figure 12(b) shows that part of this disagreement may be attributed to the nonuniform vorticity distribution of the laboratory vortices. Indeed, for interactions between vortices of similar size, i.e., $R_2/R_1>0.8$, complete merger in 1 orbit is predicted reasonably well. For vortices with more disparate sizes, however, complete merger is often achieved on a time scale much smaller than expected from the above arguments. In Sec. IV we will discuss possible reasons for this disagreement.

B. Rotating-tank experiments

In order to study the interaction between two vortices with equal radii, laboratory experiments were performed in a tank with horizontal dimensions 1.0×1.5 m that was mounted on top of a turntable. The tank was filled with water to a depth of approximately 20 cm and the flow was allowed to adjust to a solid-body rotating for at least half an hour. The angular velocity of the turntable was set to 0.7 rad s^{-1}, which corresponds to a rotation period of approximately 9.0 s. Owing to topographic vorticity production induced by the parabolic free surface,[27] cyclonic vortices tend to spiral inward toward the center of the tank, whereas anticyclonic vortices tend to spiral outward. This effect promotes cyclonic merger while inhibiting anticyclonic merger, which is the most important reason why previous rotating-tank experiments[28] revealed different merger criteria for cyclonic and anticyclonic vortices (see also the discussion in Ref. 29). In the present

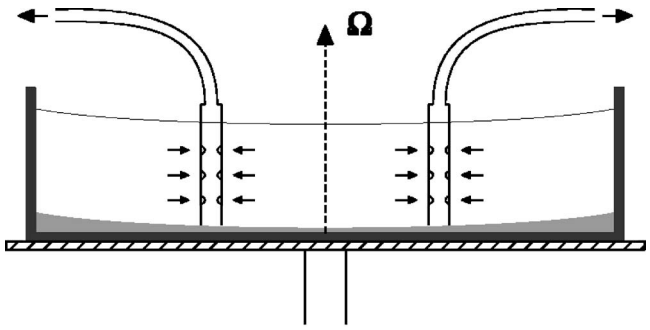

FIG. 13. Laboratory setup for the generation of two cyclonic vortices in a rotating tank.

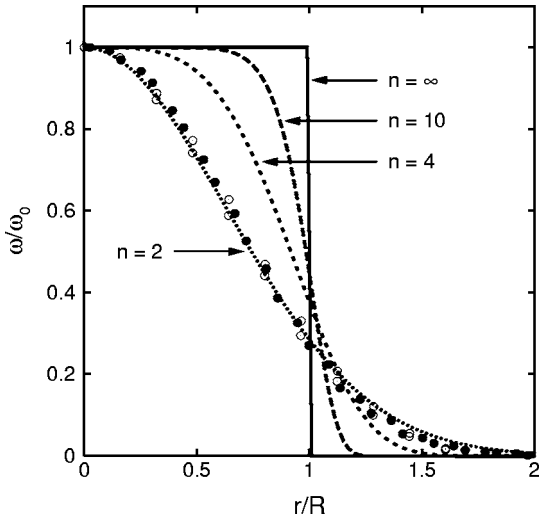

FIG. 14. Radial distributions of vorticity for two sink-induced cyclonic vortices with $\omega_2/\omega_1=0.5$. The circles and bullets correspond to the weaker and the stronger vortex, respectively. The curves represent the vorticity distributions given by Eq. (1) for different values of n.

study, the effect of the parabolic free surface was removed by introducing a parabolic-shaped bottom which mimics the shape of the free surface.

Two cyclonic vortices were created by simultaneously syphoning fluid through two perforated tubes, see Fig. 13. After the forcing was stopped, the tubes were removed and within a few rotation periods an equilibrium state was established in which the flow was cyclonically azimuthal within each vortex. The subsequent flow evolution was visualized by injecting different colours of passive dye ["fluorescein" (green) and "terasil brillant rosa" (red)] into the cores of the vortices just after the forcing was stopped. In all the experiments the dye evolved into vertical columnlike structures, which indicate that the flow is approximately two dimensional. Alternatively, the free surface was seeded with passive tracers in order to perform quantitative analyses. The flow was monitored with a video camera which was placed at some distance above the tank. The technique of particle image velocimetry[30] was used to obtain the velocity field from which the corresponding vorticity distributions could be determined.

The initial flow characteristics were controlled by variation of both the forcing period and the separation distance of the tubes. Previous laboratory experiments have shown that within the operational range of experimental parameters, these sink vortices have a circulation proportional to the volume of water withdrawn, while their radii are virtually unaffected.[28,31] Hence, cyclonic vortices with different peak vorticity and approximately equal initial radii can be generated, the peak vorticity being controlled by the amount of volume withdrawn. Figure 14 shows a typical radial cross section of the vorticity distribution of a single cyclonic vortex generated by the method described above. The measured profiles (indicated by the symbols) are close to the vorticity profile of a Gaussian vortex ($n=2$).

Figure 15 displays several dye-visualization evolutions for different initial ratios of maximum vorticity, i.e. (from top to bottom), $\omega_2/\omega_1=1.0$, $\omega_2/\omega_1=0.9$, $\omega_2/\omega_1=0.5$, and $\omega_2/\omega_1=0.2$, all with $d/\bar{R}=4.2$. In order to allow transient disturbances of the generation process to die out, the flow characteristics at $t=10T$ were taken as an initial condition. Times are indicated in the lower-right corner of each frame, with T the rotation period of the turntable, and are relative to the time at which the forcing was stopped. The vorticity evolutions are presented in Fig. 16 for the same initial conditions and may be compared with the dye-visualization evolutions in Fig. 15 since the laboratory experiments reproduced very well. The Reynolds number based on the initial circulation of the stronger vortex was about 7500.

During the initial stage of the evolution, the vortices orbit in a cyclonic sense around their common center of rotation. For identical vortices, $\omega_2/\omega_1=1.0$, each vortex acquires a pearlike shape and exchanges fluid with its neighboring vortex. Subsequently, two spiral arms are formed and at the same time the original vortex cores move toward each other to form a single axisymmetric vortex core with fluid originating from both initial vortices. Using the flow regime definitions of Sec. II, this type of interaction may be classified as complete merger. The vorticity evolution in Fig. 16 reveals that the distributions of dye and vorticity are intimately linked with each other, especially during the initial stage of the evolution. At later times, however, some differences arise because vorticity diffuses much faster than dye (in the laboratory experiments the Schmidt number is of the order of 10^3). For example, the dye distribution of the compound vortex still shows two different vortex centers, whereas only a single vortex center is present in the corresponding vorticity distribution. Also, the spirals of dye are much more pronounced than the corresponding vorticity filaments (although the latter may also be due to a lack of spatial resolution of the measurement technique). In this respect, the dye visualizations provide important information about the origin of the fluid initially within each vortex, whereas the vorticity measurements reveal whether dyed fluid may be associated with vorticity.

For slightly unequal vortices, $\omega_2/\omega_1=0.9$, the interaction process again results in complete merger, but now the exchange and shedding of dyed fluid is mainly carried by the weaker vortex. Consequently, the final vortex core contains less fluid originating from the weaker vortex than in the symmetric case. For more distinct vortices, e.g., $\omega_2/\omega_1=0.5$, and

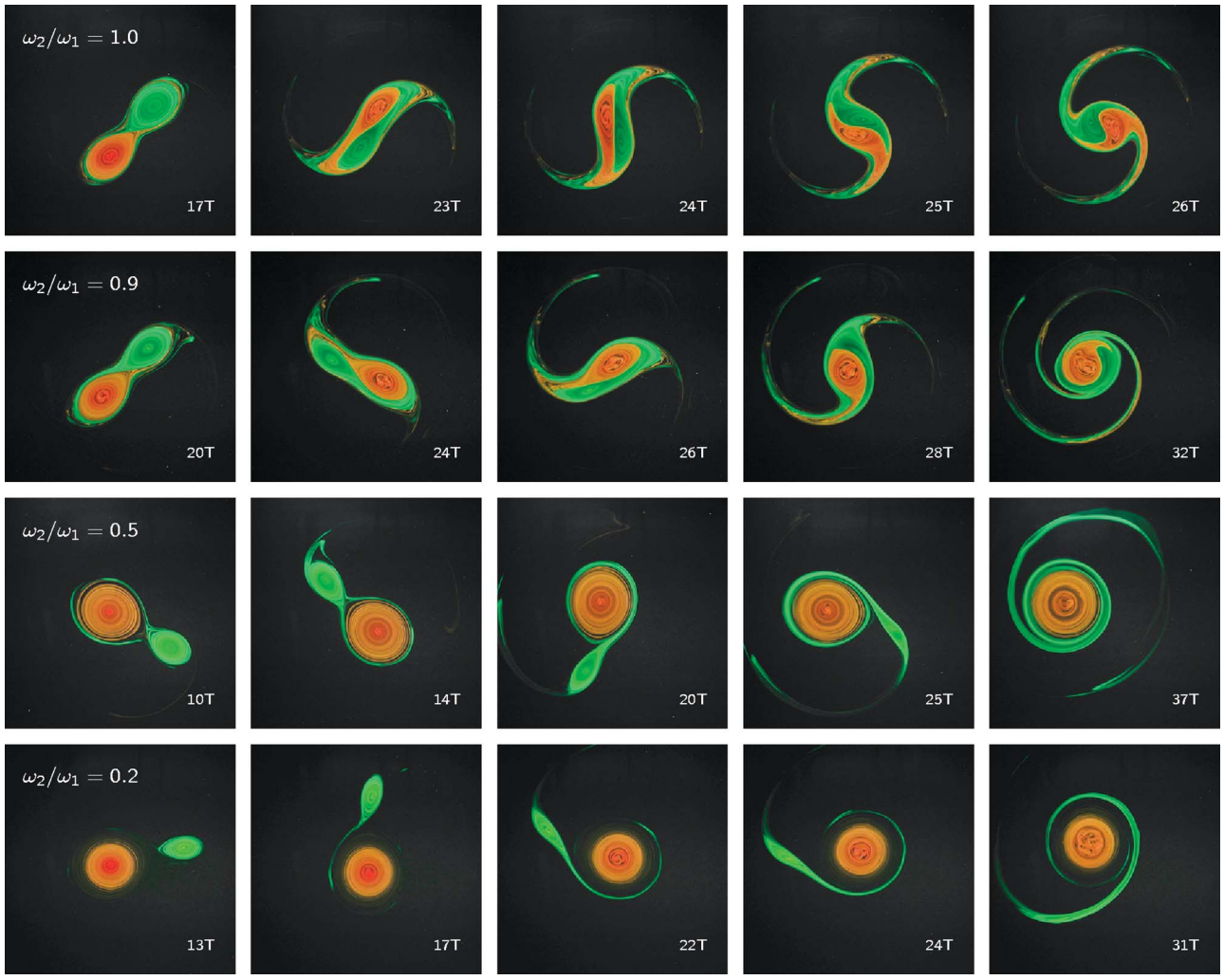

FIG. 15. (Color). Dye visualization of two cyclonic vortices in a rotating fluid for $d/\bar{R}=4.2$ and different initial ratios of maximum vorticity, i.e. (from top to bottom), $\omega_2/\omega_1=1.0$, $\omega_2/\omega_1=0.9$, $\omega_2/\omega_1=0.5$, and $\omega_2/\omega_1=0.2$, at successive times after the forcing was stopped. The tubes were separated 15 cm apart and the forcing time of the stronger vortex was 10 s. Times are indicated in the lower-right corner of each frame, with T the rotation period of the turntable. Each frame corresponds to a free-surface area of 50×50 cm^2. The stronger and weaker vortex are visualized with red and green dye, respectively.

$\omega_2/\omega_1=0.2$, the weaker vortex is completely torn apart and consequently wrapped around the stronger vortex, while the stronger vortex is virtually unaffected. The last two evolution examples have much in common with a complete straining-out event, but in practice it is difficult to distinguish between complete straining-out and complete merger. From a dynamical point of view it is only important whether the interaction results in one or two final vortices and therefore we will make no distinction between these flow regimes in the further analysis of the rotating-tank experiments.

The initial conditions of all the rotating-tank experiments are indicated by the markers in Fig. 17. As expected, all the interactions between cyclonic vortices resulted in a single vortex and no clear evidence was found for the production of a stable configuration of both a stronger and a weaker vortex. The symbols in Fig. 17 have the same meaning as in Fig. 12: filled and open symbols correspond to the production of a single final vortex in less and more than one orbit period, respectively. Also shown are the corresponding regime boundaries for inviscid interactions between equal-sized Gaussian vortices (solid lines) and the isocurve for complete merger or complete straining-out in about 1 orbit (dashed line). Again, this isocurve closely follows the critical boundary (thick solid curve) except for Gaussian vortices of similar size. Figure 17 reveals that the formation of a single vortex in one orbit is predicted well for interactions between vortices with similar peak vorticity, i.e., $\omega_2/\omega_1 \geqslant 0.7$. For smaller ratios ω_2/ω_1, however, the destruction of the weaker vortex is often achieved on a time scale much smaller than expected from the numerical simulations, similar to what was observed in the electron plasma experiments. A possible explanation for this disagreement will be given in the next section.

IV. DISCUSSION

Both electron-plasma experiments and rotating-tank experiments have shown that the times for complete merger are in reasonable agreement with inviscid dynamics when the vortices are of similar size and intensity. For more distinct vortices the weaker vortex is often destroyed on a time scale much smaller than expected from the inviscid numerical

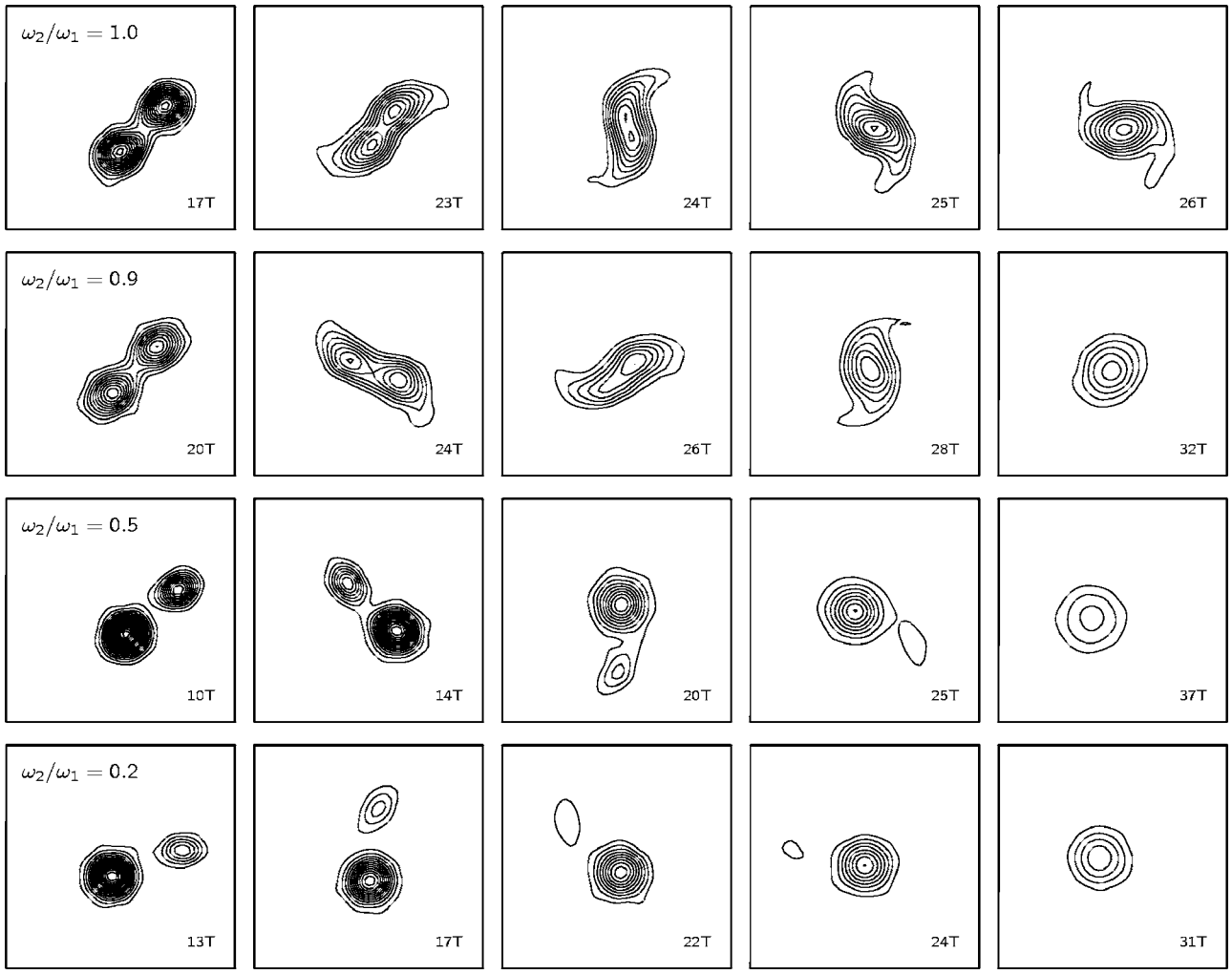

FIG. 16. Same stages of the evolution process as in Fig. 15, but now in terms of vorticity. Contour levels are drawn every 0.05 s^{-1}, starting at 0.05 s^{-1}.

simulations. Several effects may enhance the diffusive stage prior to the destruction of the weaker vortex. Nonfluid effects such as rotational and orbital pumping may gradually increase the radii of the electron vortices and thus accelerate complete merger, but these effects appear to be too weak to account for the above discrepancy.[4] Likewise, three-dimensional effects due to the presence of the Ekman boundary layer at the bottom of the rotating tank may induce an additional radial expansion of the cyclonic vortices. Although the latter effect may certainly contribute to a faster evolution toward a single final vortex, it cannot explain why weaker vortices are more quickly destroyed than stronger vortices since horizontal expansion by Ekman pumping is less important for vortices with lower peak vorticity.

Previous numerical simulations[9,22] suggest that the combined effects of horizontal diffusion and advection of vorticity may accelerate the destruction of a vortex on a time scale that is much smaller than the viscous time scale. When a vortex is placed in an external shear, low-level vorticity at the outer edge of the vortex is advected away in the form of two filaments, leaving behind an eroded vortex with a pronounced vorticity gradient on its edge.[24] In contrast to the inviscid case, low-level vorticity is constantly being regenerated along the periphery of the vortex by down-gradient smoothing. Simultaneously, the sharp vorticity gradient is preserved by the continuous shedding of low-amplitude vorticity. The joint action of stripping and diffusion causes an enhanced erosion of the vortex with a corresponding accelerated decay of peak vorticity. Eventually, the vortex is torn apart when its peak vorticity falls below a critical value associated with strength of the background shear and the initial vorticity profile of the vortex (see Sec. II).

This combined effect of stripping and diffusion is also crucial for interacting vortices, especially in regions of parameter space where inviscid calculations predict partial merger or partial straining-out of the weaker vortex core.[9] These are the flow regimes where the weaker vortex core develops steep vorticity gradients along its edge owing to the process of vortex stripping. Indeed, Figs. 12(b) and 17 show that the fast destruction of the weaker vortex occurs mainly in regions where inviscid dynamics predicts either partial merger or partial straining-out. Obviously, the weaker vortex erodes less quickly when diffusive effects become less important, i.e., when the Reynolds number based on the flow properties of the weaker vortex becomes larger. This might explain why the times for the production of a single vortex are in better agreement with inviscid dynamics for vortices of similar size or vorticity magnitude. Another reason might

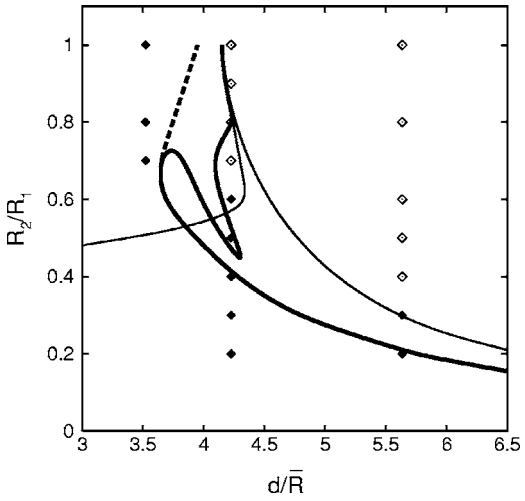

FIG. 17. Flow regime diagram of the rotating-tank experiments. Filled symbols indicate merger in less than one orbit period; open symbols indicate merger in more than one orbit period. The solid lines represent the boundaries between the numerically obtained regimes (the critical boundary is indicated by the thick solid line) and are identical to those in Fig. 3. The dashed line represents the isocurve for complete merger (or complete straining-out) in about one orbit period.

be that the formation of steep vorticity gradients by vortex stripping is largely canceled for vortices with similar circulation due to the mutual exchange of vorticity filaments.

The above reasoning is supported by Fig. 18 which shows the decay of maximum vorticity for each of the sink-induced vortices with initial ratios (a) $\omega_2/\omega_1=1.0$ and (b) $\omega_2/\omega_1=0.5$. The symbols refer to the peak vorticities of each of the vortices. The initial stage of the evolution is least-square fitted with an exponential function which closely represents the decay of each of the two vortices in isolation due to linear Ekman damping and horizontal diffusion of vorticity. For (nearly) equal vortices, the decay of maximum vorticity is virtually unaffected and the ratio ω_2/ω_1 remains close to 1 until the vortices have merged. After that, the decrease of maximum vorticity is arrested due to the larger radius of the final vortex core, i.e., larger vortices decay slower than smaller vortices owing to horizontal diffusion. For $\omega_2/\omega_1=0.5$, the peak vorticity of the weaker vortex decreases dramatically by the time that a significant amount of vorticity is ejected toward the stronger vortex, and hence the ratio of peak vorticities decreases as well until the weaker vortex is inevitably overcome by the stronger vortex. In the meantime the decay of maximum vorticity of the stronger vortex is slightly arrested due the entrainment of low-amplitude vorticity from the weaker vortex.

V. SUMMARY AND CONCLUSIONS

In this paper, we have investigated the interaction of two unequal corotating vortices both numerically and experimentally for a wide range of vorticity profiles. Inspired by previous numerical and experimental studies we considered two different cases: (a) vortices with different radii but equal peak vorticity, and (b) vortices with different peak vorticity and equal radii. Contour dynamics simulations revealed that the type of evolution depends crucially on the initial separation distance, the asymmetry of vortex properties (i.e., size and vorticity amplitude), and the steepness of the initial vorticity profile. All interaction scenarios could be classified by the same flow regimes that were used previously for interacting Rankine vortices. The effect of distributed vorticity was qualitatively the same for both equal-vorticity and equal-radii interactions.

It was found that the halo of low-amplitude vorticity strongly promotes the (partial) destruction of the weaker vortex by effectively increasing the spatial extent of each vortex. However, an alternative normalization of the separation distance, based on the second moment of vorticity, did not lead to a universal merger criterion for vortices of unequal size or unequal vorticity magnitude. The halo also promotes the vortex cores to merge more efficiently, since it accounts for a substantial part of the loss of circulation into filaments. Owing to the complexity of the filamentary structures originating from the halo, the flow regime boundaries may become very complicated and the definition of a single critical distance for the destruction of the weaker vortex may not be possible in specific regions of parameter space.

For Gaussian vortices of not too different circulation the critical boundary could be closely approximated by a criterion based on the critical distance of two identical Gaussian vortices. A similar criterion was suggested by Carnevale *et al.*[6] and Benzi *et al.*[7] in a simple punctuated Hamiltonian model of freely decaying two-dimensional flows, but in their case the criterion was based on the critical distance of two

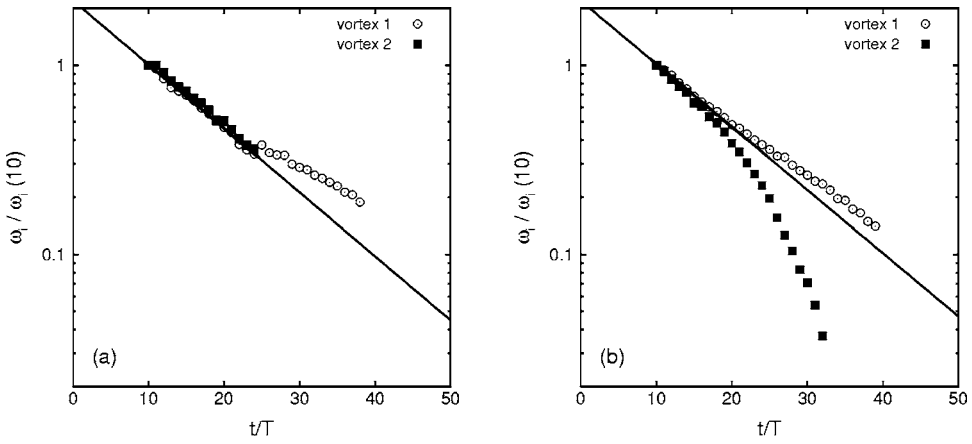

FIG. 18. Time evolution of maximum vorticity for each laboratory vortex with initial ratios of maximum vorticities (a) $\omega_2/\omega_1=1.0$ and (b) $\omega_2/\omega_1=0.5$. The initial stage of the evolution is least-square fitted with an exponential function. Time is normalized with the rotation period of the turntable, T.

equal Rankine vortices. The present study reveals that the merger criterion by Carnevale *et al.*[6] and Benzi *et al.*[7] may improve remarkably when it is based on the interaction of two Gaussian vortices. In addition, the amount of circulation bound in the larger final vortex core is largely underestimated by the transformation rule of Carnevale *et al.*[6] and Benzi *et al.*[7] and we suggest an alternative transformation rule for Gaussian vortices based on the conservation of the total initial circulation in the vortex cores, which is more applicable to vortices in moderate-*Re* two-dimensional turbulent flows.

The strong dependence of the flow regimes on the initial vorticity distribution may partly explain why previous laboratory experiments in an electron plasma show complete merger of two unequal vortices in a range of parameter space where contour dynamics simulations with uniform vorticity patches predict partial merger or partial straining-out of the smaller vortex. Since in any viscous situation all vortex interactions ultimately lead to a single vortex, we used the time required for the production of a single vortex as the relevant interaction parameter. It was shown that the measured times for complete merger are in reasonable agreement with inviscid dynamics when the vortices are very similar. For more distinct vortices the weaker vortex was often observed to be destroyed on a time scale much smaller than expected from inviscid numerical simulations. An explanation for this discrepancy was given by the combined effects of vortex stripping and viscous diffusion, which leads to an enhanced erosion of the weaker vortex. These results were verified by laboratory experiments in a conventional (rotating) fluid.

ACKNOWLEDGMENTS

We are grateful to Professor David Dritschel for providing the source code of the CASL algorithm, and to Bram Elsenaar for useful discussions and comments on an earlier version of this paper. We also would like to thank Marjolein Doorewaard for her contribution to preliminary contour dynamics simulations and laboratory experiments. One of the authors (R.R.T.) gratefully acknowledges financial support by the Royal Netherlands Academy of Arts and Sciences (KNAW).

[1] D. W. Waugh, "The efficiency of symmetric vortex merger," Phys. Fluids A **4**, 1745 (1992).
[2] D. G. Dritschel and D. W. Waugh, "Quantification of the inelastic interaction of unequal vortices in two-dimensional vortex dynamics," Phys. Fluids A **4**, 1737 (1992).
[3] I. Yasuda and G. R. Flierl, "Two-dimensional asymmetric vortex merger: Contour dynamics experiment," J. Oceanogr. **51**, 145 (1995).
[4] T. B. Mitchell and C. F. Driscoll, "Electron vortex orbits and merger," Phys. Fluids **8**, 1828 (1996).
[5] J. Jimenez, H. K. Moffatt, and C. Vasco, "The structure of the vortices in freely decaying two-dimensional turbulence," J. Fluid Mech. **313**, 209 (1996).
[6] G. F. Carnevale, J. C. McWilliams, Y. Pomeau, J. B. Weiss, and W. R. Young, "Evolution of vortex statistics in two-dimensional turbulence," Phys. Rev. Lett. **66**, 2735 (1991).
[7] R. Benzi, M. Colella, M. Briscolini and P. Santangelo, "A simple point vortex model for two-dimensional decaying turbulence," Phys. Fluids A **4**, 1036 (1992).
[8] M. V. Melander, N. J. Zabusky, and J. C. McWilliams, "Asymmetric vortex merger in two dimensions: Which vortex is 'victorious'?," Phys. Fluids **30**, 2610 (1987).
[9] H. B. Yao, N. J. Zabusky, and D. G. Dritschel, "High gradient phenomena in two-dimensional vortex interactions," Phys. Fluids **7**, 539 (1995).
[10] U. Ehrenstein and M. Rossi, "Equilibria of corotating nonuniform vortices," Phys. Fluids **11**, 3416 (1999).
[11] P. Meunier, U. Ehrenstein, T. Leweke, and M. Rossi, "A merging criterion for two-dimensional co-rotating vortices," Phys. Fluids **14**, 2757 (2002).
[12] O. U. Velasco Fuentes, "Chaotic advection by two interacting finite-area vortices," Phys. Fluids **13**, 901 (2001).
[13] M. V. Melander, J. C. McWilliams, and N. J. Zabusky, "Axisymmetrization and vorticity-gradient intensification of an isolated two-dimensional vortex through filamentation," J. Fluid Mech. **178**, 137 (1987).
[14] N. J. Zabusky, M. H. Hughes, and K. V. Roberts, "Contour dynamics for the Euler equations in two dimensions," J. Comput. Phys. **30**, 96 (1979).
[15] D. G. Dritschel, "Contour dynamics and contour surgery: Numerical algorithms for extended, high-resolution modelling of vortex dynamics in two-dimensional, inviscid, incompressible flows," Comput. Phys. Rep. **10**, 77 (1989).
[16] D. G. Dritschel and M. H. P. Ambaum, "A contour-advective semi-Lagrangian numerical algorithm for simulating fine-scale conservative dynamical fields," Q. J. R. Meteorol. Soc. **123**, 1097 (1997).
[17] B. Legras and D. G. Dritschel, "A comparison of the contour surgery and pseudo-spectral methods," J. Comput. Phys. **104**, 287 (1993).
[18] M. V. Melander, N. J. Zabusky, and J. C. McWilliams, "Symmetric vortex merger in two dimensions: Causes and conditions," J. Fluid Mech. **195**, 303 (1988).
[19] O. U. Velasco Fuentes, "Vortex filamentation: Its onset and its role on axisymmetrization and merger," Dyn. Atmos. Oceans **40**, 23 (2005).
[20] S. Kida, "Motion of an elliptic vortex in a uniform shear flow," J. Phys. Soc. Jpn. **50**, 3517 (1981).
[21] B. Legras and D. G. Dritschel, "Vortex stripping and the generation of high vorticity gradients in two-dimensional flows," Appl. Sci. Res. **51**, 445 (1993).
[22] A. Mariotti, B. Legras, and D. G. Dritschel, "Vortex stripping and the erosion of coherent structures in two-dimensional flows," Phys. Fluids **6**, 3954 (1994).
[23] D. G. Dritschel, "Vortex properties of two-dimensional turbulence," Phys. Fluids A **5**, 984 (1993).
[24] D. G. Dritschel, "Strain-induced vortex stripping," in *Mathematical Aspects of Vortex Dynamics*, edited by R. E. Caflisch (SIAM, New York, 1989), pp. 107-119.
[25] J. Weiss, "The dynamics of enstrophy transfer in two-dimensional hydrodynamics," Physica D **48**, 273 (1991).
[26] J. C. McWilliams, "The emergence of isolated coherent vortices in turbulent flow," J. Fluid Mech. **146**, 21 (1984).
[27] E. J. Hopfinger and G. J. F. van Heijst, "Vortices in rotating fluids," Annu. Rev. Fluid Mech. **25**, 241 (1993).
[28] R. W. Griffiths and E. J. Hopfinger, "Coalescing of geostrophic vortices," J. Fluid Mech. **178**, 73 (1987).
[29] G. F. Carnevale, P. Cavazza, P. Orlandi, and R. Purini, "An explanation for anomalous vortex merger in rotating-tank experiments," Phys. Fluids A **3**, 1411 (1991).
[30] R. J. M. Bastiaans, "Cross-correlation PIV: Theory, implementation and accuracy," Technical Report, Eindhoven University of Technology (2000).
[31] R. R. Trieling, A. H. Linssen, and G. J. F. van Heijst, "Monopolar vortices in an irrotational annular shear flow," J. Fluid Mech. **360**, 273 (1998).